# Structural Behaviour of Slender Geopolymer Concrete Beams Without Stirrups

Jiandong Lu[1](✉), Yuguang Yang[1], Herbert van der Ham[1,2], and Danny Fu[2]

[1] Delft University of Technology, Delft, The Netherlands
J.Lu-1@tudelft.nl
[2] Boskalis Nederland B.V., Papendrecht, The Netherlands

**Abstract.** Geopolymer concrete is a new alternative material to conventional concrete with less carbon dioxide emissions. Researchers have reported much research on the material properties of geopolymer concrete. However, research on the behaviour of this new material at the structural level is still limited, especially at a full-scale structural level. Three geopolymer concrete beams with a total height of 700 mm were tested till the shear failure. The first two specimens were subjected to the monotonically increasing load until the shear failure. The third specimen was first loaded under sustained load at the level of 80 kN for three weeks to investigate the influence of shrinkage and creep on the cracking behaviour. Then the specimen was then unloaded and reloaded again to failure. Digital Image Correlation (DIC) measurement was used to measure the surface deformation of the whole span of the beam. The crack spacing, crack width and crack development were investigated using the DIC measurement. The experimental results showed that the shear capacity of tested geopolymer concrete beams is lower than the calculated result based on the Eurocode.

**Keywords:** Full-scale test · Geopolymer concrete · Shear behaviour in beams without stirrups · Digital image correlation

## 1 Introduction

Geopolymer concrete is environmentally friendly and sustainable because it produces a lower carbon footprint than conventional concrete. Besides, it can utilise industrial waste materials, such as fly ash and blast furnace slag. Therefore, increasing interest has been forwarded to geopolymer concrete over the past few years. Many researchers have investigated the material regarding its mechanical properties and composition [1–3]. Compared to the mechanical properties, a relatively small amount of investigations [4–7] was carried out at the structural level, especially for the shear capacity of large-scale specimens. In terms of engineering applications, a pilot prestressed bicycle bridge made of geopolymer concrete was implemented in 2022 in the Netherlands. The design of the structure was verified by tests on small-scale prestressed geopolymer concrete beams carried out in the Stevin II lab, and the results were reported in Lit. [9]. However, applications of geopolymer concrete for real-world structures still have to follow


A. Ilki et al. (Eds.): *fib* Symposium 2023, LNCE 350, pp. 835–845, 2023.
https://doi.org/10.1007/978-3-031-32511-3_86

the principle of design assisted by tests because of the lack of dedicated codes. More specifically, information on the cracking behaviour and shear capacity considering the size effect in reinforced geopolymer concrete members is unclear.

In this paper, the presented test series are related to the design requirement of the concrete slabs of a tunnel entrance in the Netherlands using this type of geopolymer concrete. Because no design rules are available in Eurocode on the cracking behaviour and shear design of geopolymer concrete structures, it was decided to test three full-scale structures to investigate their cracking behaviour and shear capacity. The structural behaviour of the geopolymer concrete beams, including the shear capacity, crack width, and spacing, was evaluated. The experimental results were compared to the existing models for ordinary concrete, including the current Eurocode and ACI 318–19.

## 2 Test Program

### 2.1 Material

The specimens use a commercialised geopolymer concrete mixture in the Netherlands from the concrete provider A. Jansen B.V. [8]. The aggregates were recycled from the tar-containing asphalt granulate through thermal processing. The maximum aggregate size used in this concrete is 16 mm. The compositions of the geopolymer concrete are listed in Table 1. The detailed information mixture design of the geopolymer concrete used in this paper can be referred to as Lit. [9]. The mean 28-day cubic compressive strength is 42.1 MPa, the splitting tensile strength is 4.5 MPa, and the elastic Young's modulus is 24 GPa.

**Table 1.** Mixture design [9].

| Component | RaMaC C33/43 [kg/m3] |
|---|---|
| Course aggregates | 759 |
| Fine aggregates | 715 |
| Precursors (blast furnace slag, fly ash) | 600 |
| Activators | 106 |
| Additives | 0.6 |
| Water | 151 |

### 2.2 Test Specimen and Measurement Layout

Figure 1 and Table 2 show the details of the specimen. In total, three beams were tested. The total length of the specimen is 8 m, and the cross-section size is 0.7 m x

0.3 m. Some width inconsistencies in the longitudinal direction were observed during the casting process. Therefore, the average width around the mid-span is listed in Table 2. As for reinforcement, the cross-section was reinforced by 3Ø25 at the bottom and 2Ø25 at the top. The concrete cover was 60 mm. Therefore, the corresponding effective height $d$ was 627.5 mm, and the shear span ratio $a/d$ was 3.98. Additional shear reinforcement was added locally outside the supports to avoid anchorage failure.

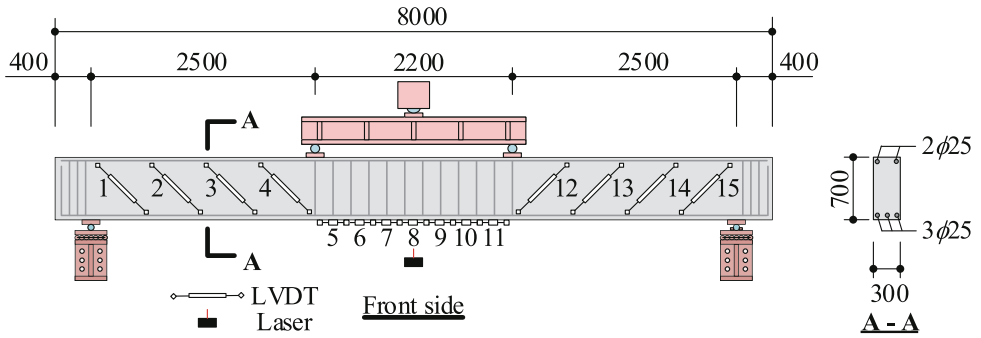


**Fig. 1.** Schematic configuration of the loading test setup and sensor layout (unit: mm).

**Table 2.** Detailed information on the specimens.

| Specimens | Shear span [m] | Longitudinal reinforcement ratio [%] | Average mid-span width [mm] | $a/d$ [-] | Loading type |
|---|---|---|---|---|---|
| A1 | 2.5 | 0.78 | 321 | 3.98 | Short term |
| A2 | 2.5 | 0.78 | 292 | 3.98 | Short term |
| A3 | 2.5 | 0.78 | 289 | 3.98 | Long term |

Four-point bending test was carried out in this experimental campaign. The load was applied by displacement-control method, and the loading rate was 0.01 mm/s. Specimens A1 and A2 were loaded with an increment of 10 kN until the load reached 100 kN. Then, the specimen was unloaded to 5 kN and reloaded with an increment of 20 kN. After reaching 180 kN, the load level was increased continuously until failure. While for specimen A3, the load level was kept constant for three weeks at 80 kN. Then, the specimen was unloaded and reloaded until failure.

For the measurement, 15 LVDTs were used on the front side of the specimen. Eight of them were glued on the side surface to measure the opening of the flexural-shear cracks in the constant shear force region, and the rest were glued in the middle on the bottom surface to measure the opening of the flexural cracks in the pure bending zone. The gauge length of the LVDTs on the bottom surface is 300 mm. For the LVDTs on the side surface, the gauge length is 750 mm, and the angle is 45 degrees to the horizontal direction. One laser sensor was installed underneath the mid-span location to measure the deflection. On the back side, three cameras were used to perform the 2D Digital Image Correlation (DIC) to cover the whole span of the specimen. The 2D DIC analysis

was performed in the commercial software GOM [10]. The subset size of 19 pixels and the step size of 16 pixels were used in the analysis.

# 3 Results

## 3.1 Load-Displacement Curves

Figure 2 depicts the load-displacement curves of the three specimens. It should be mentioned that the measurement during the unloading stage of specimen A3 was not recorded, and the reading from instruments was reset before the reloading stage of specimen A3. The average unloading stiffness from specimens A1 and A2 was used to estimate the residual deformation of specimen A3, and the measurement from the reloading stage was reconnected to the previous stage. Overall, The specimen stiffness decreased after the initial cracking and remained constant until failure. As expected, the initial stiffness of specimen A1 is slightly larger than the other two specimens because of the varied width. However, the width in the constant shear force zone of the three specimens was close to 300 mm, leading to comparable shear capacities.

Table 3 summarises the experimental results. The failure shear force was determined at the cross-section in the middle of the critical shear crack. The self-weight of the specimen was also considered. According to the results, the sustained load did not significantly impact the failure load compared to the other two specimens. The failure load of specimen A3 was even 5.8% higher than that of the specimens subjected to monotonic load.

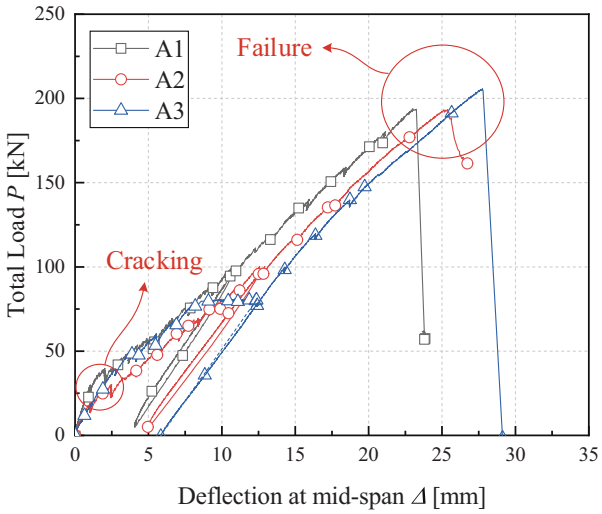


**Fig. 2.** Load-displacement curves.

**Table 3.** Summary of test results.

| Specimens | *a/d* [-] | Cracking load $P_{cr}$ [kN] | Failure load $P_{failure}$ [kN] | Failure deflection $\Delta_{failure}$ [mm] | Failure shear force $V_{failure}$ [kN] |
|---|---|---|---|---|---|
| A1 | 3.98 | 29.7 | 193.6 | 23.2 | 107.6 |
| A2 | 3.98 | 28.9 | 193.0 | 25.3 | 104.6 |
| A3 | 3.98 | 28.9 | 205.8 | 27.8* | 114.4 |

* A residual deformation of 5.8 mm was assumed according to the average unloading stiffness.

### 3.2 Crack Pattern and Failure Mode

Typical flexural-shear failure was observed in the three tests. Since the structural behaviours of the three specimens are similar, only the results of specimens A1 and A3 were explained in detail.

Figure 3a shows the failure crack pattern on the DIC side, and Fig. 3b shows the maximum principal strain field of the DIC results just before failure. As shown in Fig. 3b, the secondary crack of the critical shear crack started to develop at the level of the longitudinal reinforcement. At the same time, the top part of the critical shear crack propagated gradually toward the compressions zone with an angle of 40 degrees. Just before the failure, the critical shear crack merged with the top part of crack 1, resulting in an unstable crack propagation toward the loading point and the support. The unstable propagation caused a very brittle flexural-shear failure.

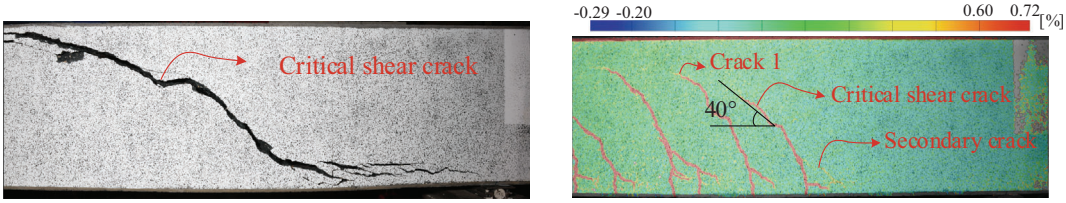


**Fig. 3.** Crack pattern of specimen A1 on the DIC side: (a) final failure crack pattern; (b) maximum principal strain field of DIC close to failure ($P = 191.9$ kN, $P_{failure} = 193.1$ kN)

### 3.3 Crack Width and Crack Spacing at Longitudinal Reinforcement Level

#### 3.3.1 Specimen A1

The crack width development of a single crack was measured by the DIC at several load stages. Before further interpretation of the measured crack width, the DIC analysis should be verified first. The results of LVDTs were used to make the verification. Three virtual strain gauges were set in GOM according to the locations of LVDT 05 to 08. Figure 4 shows the comparison between the DIC and LVDT results. If the measurement of a single LVDT was compared, the results started to deviate from the diagonal line

as the measurement increased. The variation of crack location in the width direction might cause the derivation. Therefore, the results of neighbour LVDT were summed, for example, LVDT 05 and 06, to make the comparison. After the summation, the results were less deviated and within the range of 15% error, which verified the accuracy of the DIC measurement.

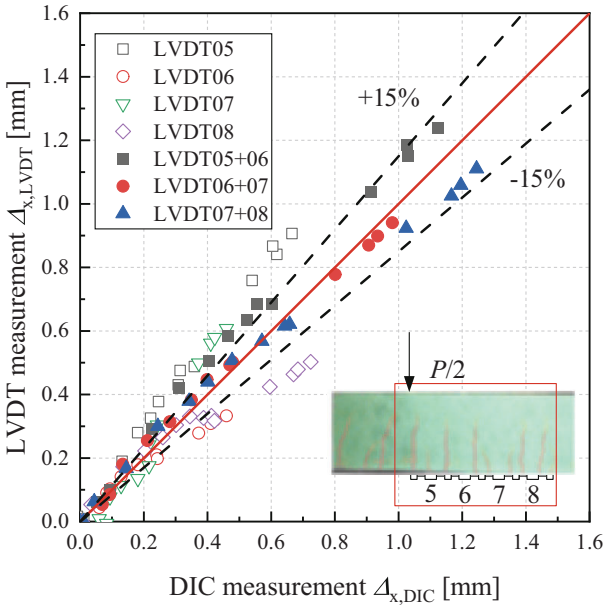


**Fig. 4.** Comparison between LVDT and DIC measurement at the pure bending zone.

Figure 5 shows the crack pattern and spacing in the pure bending zone when the load was 191.9 kN. The flexural cracks developed evenly in the pure bending zone, and the average spacing was 154 mm. The maximum crack spacing was observed between cracks #2 and #3, which was 249 mm.

Eight major flexural cracks were selected for further analysis of crack width development. Virtual LVDTs with a length of 50 mm were manually set at the longitudinal reinforcement level in GOM to measure the crack width development of each major flexural crack. Figure 6 presents the width development of each crack at some selected instants. When the load was 40 kN, five cracks developed simultaneously. Then, the

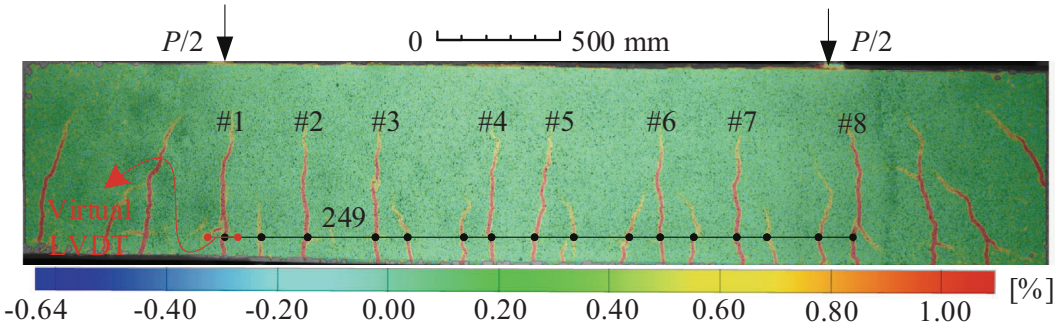


**Fig. 5.** Maximum principal strain field in the pure bending zone at $P = 191.9$ kN.

crack width increased stably as the load increased. The maximum crack width was around 0.41 mm, which occurred in cracks#5 and #8.

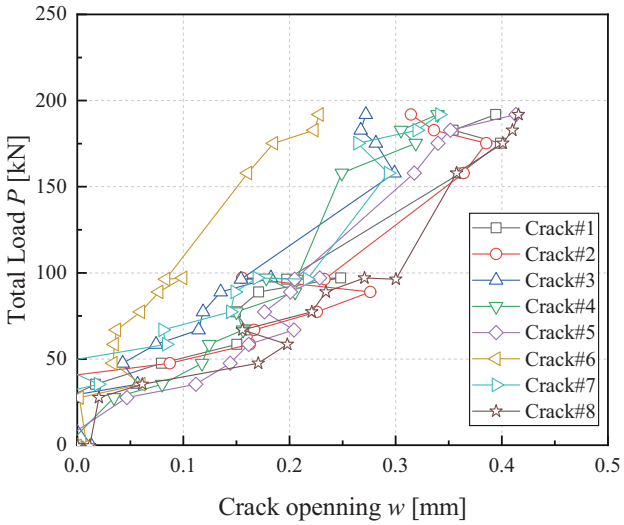


**Fig. 6.** Crack opening development of major flexural cracks in the pure bending zone

### 3.3.2 Specimen A3

For specimen A3, the sustained load was applied to investigate the time effect on the crack width development. Figure 7a presents the measurements of LVDTs 05 to 11, which were placed within the pure bending zone. The original point was the instant when the load reached 80 kN. Except for LVDT 07, all the measurements increased gradually against time. One possible reason is that a crack developed at the connection point of LVDTs 07 and 06. The average result of those two LVDTs was indicated by a black dashed line, which showed a very comparable tendency to other measurements. The deformation increased by around 24.6% after the sustained loading. Figure 7b shows the cumulative deformation curves as a function of time. Despite the fluctuation in the measurement, the results showed that half of the total incremental deformation developed within the first eight days. Then, the increasing rate of the deformation decreased and became more steady. However, the deformation was still increasing and did not stabilise after the 25-day sustained load.

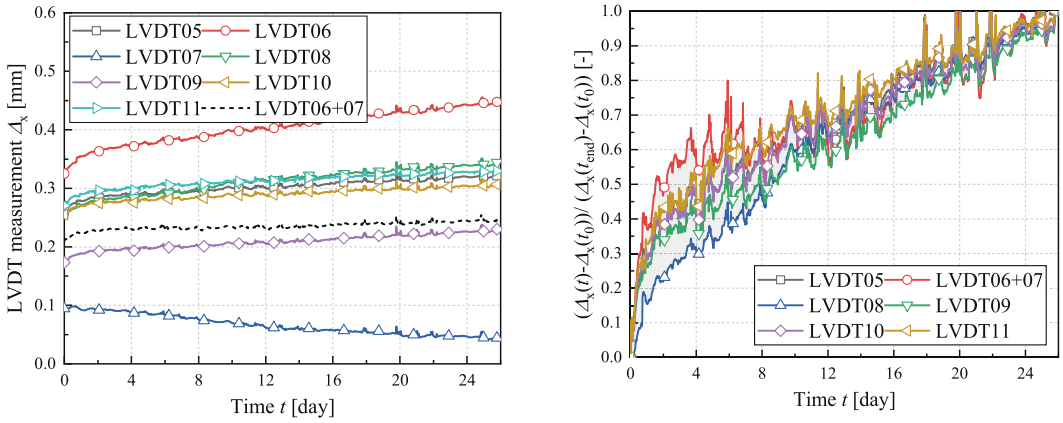


**Fig. 7.** Measurements of LVDTs 05 to 08: (a) elongation development against time; (b) cumulative deformation curve.

# 4 Discussion

## 4.1 Crack Width and Spacing Calculation

Since the structural behaviour of geopolymer concrete members is still under investigation, the applicability of the current Eurocode [11] for this new type of concrete is unclear. The experimental results of flexural cracking behaviour were compared to the calculated results from the current Eurocode. In the crack width calculation, the coefficient $k_t$ used in the Eurocode formula (7.9) was adopted as 0.6 to consider the short-term loading effect. The calculated crack width under the load of 191.9 kN was 0.41 mm, which was quite comparable to the maximum measured crack width. As for the crack spacing, the Eurocode formula (7.11) was used, and the result was 347 mm, much larger than the experimental result (i.e., 249 mm). The comparison shows that the current Eurocode is applicable to capture the crack opening for this type of geopolymer concrete, although the crack spacing was overestimated.

## 4.2 Shear Capacity Calculation

The experimentally obtained shear capacity of the three geopolymer concrete beams was compared with the prediction of the current Eurocode [11] shear formula, the ACI-318 [12], the Critical Shear Crack Theory (CSCT) [13], and the Critical Shear Displacement Theory (CSDT) [14]. Table 4 summarises the experimental and calculated results. In general, all four models overestimated the shear capacity of the specimen. The ACI and CSDT models gave a closer prediction. One possible explanation for the overestimation is the cracked surface roughness. Figure 8 shows the cracked surface of a cube after the splitting tensile test. The cracked surface went through almost all the aggregates, similar to the cracked surface of a high-strength concrete specimen. The aggregates used in this concrete were recycled from asphalt through thermal processing. The thermal processing might induce some internal micro-cracks of the aggregates, resulting in a lower aggregate strength. Therefore, a relatively smooth cracked surface was formed

after cracking, contributing less aggregate interlock force. The surface roughness index $R_s$ proposed by Lange et al. [15] was used in this paper, which is the ratio between the measured surface area and the projected area in the X-Y plane. The average $R_s$ of two cubes was 1.064, comparable to the measurement of high-strength concrete by Perera and Mutsuyoshi [16]. As Yang et al. [17] suggested, a reduction factor $R_a$ of 0.75 can be used to consider the less aggregate interlock contribution for high-strength concrete. The reduction factor was used to re-evaluate the shear capacity based on CSDT, and the modified results are closer to the experimental results.

**Table 4.** Comparison between experimental and theoretical shear capacity.

| Specimens | $V_{failure}$ [kN] | $V_{EU}$ [kN] | $V_{ACI}$ [kN] | $V_{CSCT}$ [kN] | $V_{CSDT}$ [kN] | $V_{CSDT,mo}$ [kN] |
|---|---|---|---|---|---|---|
| A1 | 107.6 | 132.5 | 109.4 | 129.6 | 121.9 | 108.2 |
| A2 | 104.6 | 132.5 | 109.4 | 129.6 | 121.9 | 108.2 |
| A3 | 114.4 | 132.5 | 109.4 | 129.6 | 121.9 | 108.2 |

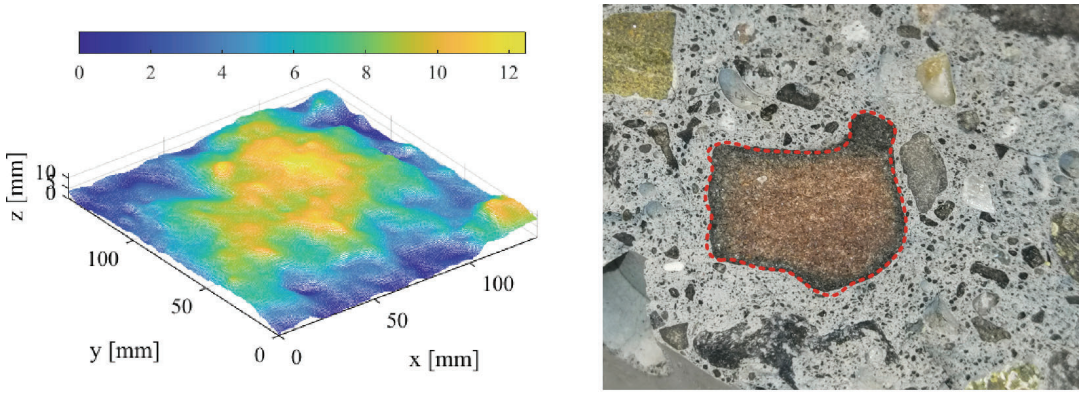


**Fig. 8.** Cracked surface of a cube after splitting tensile test: (a) 3D scanning results; (b) breakage of an aggregate (dashed line)

## 5 Conclusions

This paper presents the results of the four-point bending tests performed on three reinforced geopolymer concrete beams. The typical flexural-shear failure was observed in all specimens. With the help of the DIC, the crack width and spacing were further analysed. The experimental results were compared to several existing evaluation methods. Some conclusions and recommendations can be summarised as follows.

1) The three-week sustained load did not impact the shear capacity significantly. The shear capacity of specimen A3 was 114.4 kN, which was higher than the capacity of the specimens subjected to monotonic load.

2) The crack opening increased by around 24.6% during the sustained loading. More than 50% deformation was developed within the first eight days. However, the deformation did not stabilise at the end of the sustained loading. A sustained loading test with a more extended period is still needy.
3) The calculated crack width for flexural cracks based on the current Eurocode was comparable to the experimental results, proving the applicability of the current Eurocode in this type of geopolymer concrete.
4) The shear strength formula in ACI 318–19 can give the best prediction of the shear capacity of the specimens, while other formulae overestimate the shear capacity. The relatively smooth cracked surface indicated that the recycled aggregate might have lower strength. Therefore, less aggregate interlock contribution should be considered during the design phase.

## References

1. Singh B, Ishwarya G, Gupta M, Bhattacharyya SK (2015) Geopolymer concrete: A review of some recent developments. Constr Build Mater 85:78–90
2. Pilehvar S et al (2018) Physical and mechanical properties of fly ash and slag geopolymer concrete containing different types of micro-encapsulated phase change materials. Constr Build Mater 173:28–39
3. Zhang P, Gao Z, Wang J, Guo J, Hu S, Ling Y (2020) Properties of fresh and hardened fly ash/slag based geopolymer concrete: a review. J Clean Prod 270:122389
4. Kathirvel P, Kaliyaperumal SRM (2016) Influence of recycled concrete aggregates on the flexural properties of reinforced alkali activated slag concrete. Constr Build Mater 102:51–58
5. Yacob NS, ElGawady MA, Sneed LH, Said A (2019) Shear strength of fly ash-based geopolymer reinforced concrete beams. Eng Struct 196:109298
6. Ozturk M, Arslan G (2022) Shear behavior of granulated blast furnace slag-based geopolymer-reinforced concrete beams. Buildings 12(12):2053
7. Albidah AS (2023) Shear behviour of metakaolin-fly ash based geopolymer concrete deep beams. Eng Struct 275:115271
8. van der Ham H, Janssen T (2022) Prestressed geopolymer concrete bridge with 100% secondary aggregates. 6th fib International Congress on Concrete Innovation for Sustainability. The International Federation for Structural Concrete, Oslo, pp 2419–2428
9. Jansen A, Beton BV. https://www.ajansenbv.com
10. GOM. GOM Correlate Professional (2018). https://www.gom.com/en/products/gom-suite/gom-correlate-pro
11. British Standards I (2004) Eurocode 2: design of concrete structures. British Standards Institution, London
12. ACI Committee. (2019). ACI 318–19: Building Code Requirements for Structural Concrete and Commentary. American Concrete Institute: Farmington Hills, MI, USA
13. Muttoni A, Fernández Ruiz M (2008) Shear strength of members without transverse reinforcement as function of critical shear crack width. ACI Struct J 105:163–172
14. Yang Y (2014) Shear behaviour of reinforced concrete members without shear reinforcement. Delft University of Technology, Delft
15. Lange DA, Jennings HM, Shah SP (1993) Relationship between fracture surface roughness and fracture behavior of cement paste and mortar. J Am Ceram Soc 76(3):589–597
16. Perera SVT, Mutsuyoshi H (2013) Shear behavior of reinforced high-strength concrete beams. ACI Struct J 110(1)

17. Yang Y, den Uijl J, Walraven J (2016) Critical shear displacement theory: on the way to extending the scope of shear design and assessment for members without shear reinforcement. Struct Concr 17(5):790–798